Agricultural and Forest Meteorology 211 (2015) 115–127

Contents lists available at ScienceDirect

Agricultural and Forest Meteorology

journal homepage: www.elsevier.com/locate/agrformet

Secondary circulations at a solitary forest surrounded by semi-arid shrubland and their impact on eddy-covariance measurements

Fabian Eder[a,b,*], Frederik De Roo[a], Eyal Rotenberg[c], Dan Yakir[c], Hans Peter Schmid[a], Matthias Mauder[a,b]

[a] Institute of Meteorology and Climate Research, Atmospheric Environmental Research (IMK-IFU), Karlsruhe Institute of Technology (KIT), Kreuzeckbahnstrasse 19, 82467 Garmisch-Partenkirchen, Germany
[b] Institute of Geography and Geoecology (IfGG), Karlsruhe Institute of Technology (KIT), Kaiserstraße 12, 76131 Karlsruhe, Germany
[c] Department of Earth and Planetary Sciences (EPS), The Weizmann Institute of Science, Rehovot 76100, Israel

ARTICLE INFO

Article history:
Received 4 December 2014
Received in revised form 26 May 2015
Accepted 1 June 2015

Keywords:
Eddy covariance
Large-eddy simulation
Lidar
Ogive analysis
Secondary circulation

ABSTRACT

The Yatir forest in Israel is a solitary forest at the dry timberline that is surrounded by semi-arid shrubland. Due to its low albedo and its high surface roughness, the forest has a strong impact on the surface energy budget, and is supposed to induce a secondary circulation, which was assessed using eddy-covariance (EC) and Doppler lidar measurements and large-eddy simulation (LES). The buoyancy fluxes were 220–290 W m^{-2} higher above the forest, and the scale of the forest relative to the boundary-layer height is ideal for generating a secondary circulation, as confirmed by a LES run without background wind. However, usually a relatively high background wind (6 m s^{-1}) prevails at the site. Thus, with the Doppler lidar a persistent updraft above the forest was detected only on 5 of the 16 measurement days. Nevertheless, the secondary circulation and convective coherent structures caused low-frequency flux contributions in the mixed-layer w spectra, the surface layer u and w spectra and in the surface-layer momentum fluxes. According to the ogive functions from the tower data and a control volume approach using the LES, such low-frequency contributions with timescales >30 min were a major reason the non-closure of the energy balance at the desert site. In the roughness sublayer above the forest, these large structures were broken up into smaller eddies and the energy balance was closed.

1. Introduction

The convective atmospheric boundary layer is conceptually divided into a surface layer and a mixed layer or outer layer (Driedonks and Tennekes, 1984). The turbulence of the homogeneous surface layer under stationary convective conditions obeys Monin–Obukhov similarity theory. In addition, large convective coherent structures that scale with the height of the atmospheric boundary layer influence the horizontal wind component (Kaimal, 1978; Højstrup, 1981). They are often called 'inactive motions' because according to Townsend (1961) and Bradshaw (1967) they are imprints of large turbulent fluctuations originating from the outer layer and do not contribute to shear stress. The convective coherent structures are thermals (Wilczak and Tillman, 1980; Williams and Hacker, 1993), open cells (Kropfli and Hildebrand, 1980; Träumner et al., 2014) or, in case of background wind, as horizontal rolls (Etling and Brown, 1993; Drobinski et al., 1998; Maronga and Raasch, 2013) and typically have horizontal length scales of 1.5 times the boundary-layer height (Kaimal et al., 1976; Caughey and Palmer, 1979; Liu et al., 2011). However, homogeneous field conditions can rarely be met in reality, which complicates the application of universal scaling rules and the interpretation of boundary-layer measurements. Differences in surface roughness, temperature or moisture are supposed to create internal boundary layers (Garratt, 1990; Strunin et al., 2004), to induce advection on the surface-layer or boundary-layer scale (Raupach and Finnigan, 1995; Higgins et al., 2013) and, if the differences in surface properties are strong enough and if the surface patches are large enough, to induce secondary circulations (Mahfouf et al., 1987; Dalu and Pielke, 1993; Courault et al., 2007; van Heerwaarden and Vilà-Guerau de Arellano, 2008; Garcia-Carreras et al., 2010; Sühring and Raasch, 2013; Dixon et al., 2013; Kang and Lenschow, 2014; van Heerwaarden et al., 2014).

* Corresponding author at: Institute of Meteorology and Climate Research, Atmospheric Environmental Research, Karlsruhe Institute of Technology, Kreuzeckbahnstraße 19, 82467 Garmisch-Partenkirchen, Germany. Tel.: +49 8821 183 137; fax: +49 8821 73573.
E-mail address: fabian.eder@kit.edu (F. Eder).

http://dx.doi.org/10.1016/j.agrformet.2015.06.001
0168-1923/

Large-scale boundary-layer structures also have an effect on surface flux measurements conducted with the eddy covariance technique (Foken, 2008; Foken et al., 2011). The eddy-covariance (EC) method is very attractive for determining land-atmosphere exchange of energy and traces gases, since it does not disturb the ecosystem under investigation and the flux measurement operates on the ecosystem scale, i.e. it is representative of a larger area (Schmid, 1994; Baldocchi, 2003). However, this method generally does not close the energy balance at the earth's surface, which is called the energy balance closure problem (Foken, 2008). Accordingly, the energy balance ratio R, which is the sum of sensible heat flux Q_H and latent heat flux Q_E divided by net radiation $-Q_S{}^*$ minus the ground heat flux Q_G,

$$R = \frac{Q_H + Q_E}{-Q_S{}^* - Q_G}, \tag{1}$$

is usually smaller than unity. Multi-site analyses across different ecosystems have shown that energy balance ratios usually range between 0.7 and 0.9 (Wilson et al., 2002; Hendricks-Franssen et al., 2010; Stoy et al., 2013).

A potential reason for this is the non-consideration of fluxes carried by (i) turbulent structures with timescales larger than the averaging time of the EC system (Sakai et al., 2001; Turnipseed et al., 2002; Foken et al., 2006; Charuchittipan et al., 2014) or by (ii) secondary circulations that are bound to surface heterogeneities and do not move in space (Lee and Black, 1993; Mahrt, 1998; Hiyama et al., 2007). There are indications that the non-closure of the energy balance is related to the heterogeneity of the surrounding landscape (Mauder et al., 2007a; Panin and Bernhofer, 2008; Stoy et al., 2013), but experimental evidence that secondary circulations are an important transport mechanism in the surface layer is still lacking.

In this study, we aim to investigate the structure of the convective boundary layer above a well-defined surface heterogeneity. The Yatir forest in Israel is a planted pine forest with a scale of approximately 6–10 km, located in a semi-arid region at the dry timberline at the northern border of the Negev desert. Due to its low albedo and its increased surface roughness as compared to the semi-arid desert, the forest generates higher turbulent heat fluxes than the adjacent desert (Rotenberg and Yakir, 2011). We hypothesize that the resulting spatial differences in surface buoyancy flux,

$$Q_B = Q_H\left(1 + 0.61T\frac{c_p Q_E}{\lambda Q_H}\right), \tag{2}$$

where T is the temperature, c_p is specific heat of air at constant pressure and λ is the heat of vaporization (Schotanus et al., 1983; Charuchittipan et al., 2014), should drive a secondary circulation between the forest and the desert. For this reason, it will be investigated whether Yatir forest is large enough and whether the surface heat flux differences are strong enough to modify the convective boundary-layer dynamics and to induce a secondary circulation. Scaling approaches, ground-based remote sensing measurements, high-frequency 3d-wind measurements and large-eddy simulation (LES) will be used for this study. In particular, the role of secondary circulations for the measured surface energy balances at the forest and the desert site will be investigated. It is intended to provide evidence why the turbulent heat fluxes are likely to be underestimated by the EC method. For this purpose, wind spectra and ogive functions will be calculated and the LES model will be used to identify the missing flux components by considering the flux budget equation of virtual control volumes.

2. Methods

2.1. Research site

The measurements (Fig. 1) were taken at Yatir pine forest (31°20′43.1″N, 35°3′6.7″ E, 660 m a.s.l.) and in the nearby semi-arid shrub land (31°19′6.5″N, 34°58′54.84″E, 461 m a.s.l.). The site lies in the transition zone between the Mediterranean climate and the semiarid climate. The mean annual precipitation is 285 mm with a distinct dry summer period. The measurement campaign lasted from 21 August to 11 September 2013. As such, it took place more than 6 months after the last rain event in the area.

The Yatir forest is dominated by *Pinus halpensis* trees of 11 m height that were planted mostly from 1964 to 1969 and cover an area of about 2800 ha (Grünzweig et al., 2003; Rotenberg and Yakir, 2011). The surrounding area has been under grazing for at least several decades and is sparsely covered with shrubs and herbaceous annuals and perennials. Since the measurements were conducted at the end of the dry season, the major part of the semi-arid shrub-

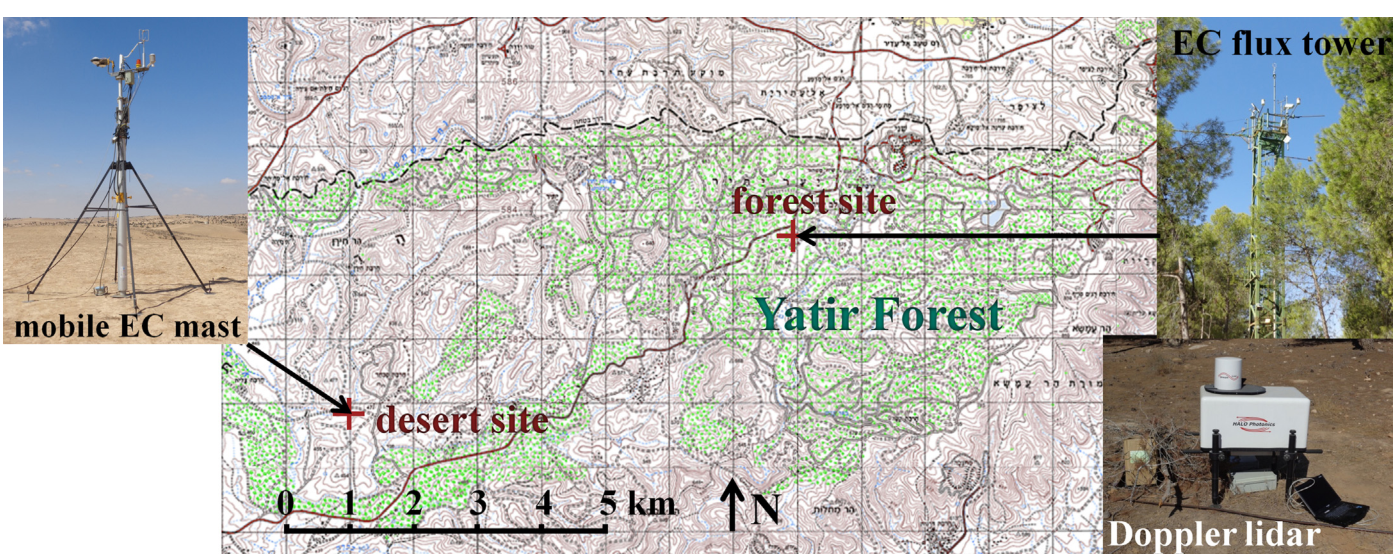

Fig. 1. Topographic map of the Yatir forest showing the locations of the measurement devices at the desert site and the forest site. Please note that there is no forest south and west of the desert site at present.

land was free of vegetation. For this reason, we will call the site that was located there a "desert" for simplicity.

The atmospheric boundary layer in the region is known to be influenced by cyclical large-scale synoptic weather variations (Dayan et al., 1988). The weather conditions during summer are dominated by the "Persian trough", a surface low-pressure trough that extends from the Asian monsoon region through the Persian Gulf to the Aegean Sea (Ziv et al., 2004). It is responsible for the persistent north-westerly flow from the eastern Mediterranean to Israel, known as the Etesian winds. The Persian trough is capped by a subtropical anticyclone centred over North Africa and the Middle East, and the strength of that anticyclonic flow determines the depth of the trough and the mean boundary-layer depth in the region (Dayan et al., 2002). Furthermore, the boundary-layer development is also affected by the diurnal sea-breeze cycle. During daytime, a sea breeze from the Mediterranean Sea that acts like a weak cold front penetrates inland (Dayan et al., 1988; Dayan and Rodnizki, 1999). It is associated with a reduced boundary-layer depth (Levi et al., 2011).

2.2. Eddy-covariance and radiation measurements

In order to assess the energy balance and the turbulent heat fluxes at the forest site and the desert site, EC and radiation measurements were conducted. At the forest, data from the FLUXNET station "Yatir" (IL-Yat) were used (Fig. 1). A R3-50 sonic anemometer (Gill Instruments, UK) measured the wind vector and the sonic temperature, a LI-7000 gas analyzer (LiCOR Biogeosciences, USA) the water vapour and carbon dioxide concentration, two CM21 pyranometers (Kipp & Zonen, The Netherlands) the short-wave up- and down-welling radiation and two PIR pyrgeometers (Eppley lab, USA) the long-wave up- and down-welling radiation. The sonic and the inlet of the gas analyzer were mounted at a height of 19 m a.g.l., i.e. 8 m above the top of the forest canopy, the radiation sensors at 5 m above the top of the forest (Rotenberg and Yakir, 2011). The data were stored on a CR1000 data logger (Campbell Scientific, USA). In the desert, a small meteorological mast was operated (Fig. 1) that was equipped with a R3-100 sonic anemometer (Gill Instruments, UK), a LI-7200 gas analyzer (LiCOR Biogeosciences, USA), two CMP21 pyranometers (Kipp & Zonen, The Netherlands), two CGR4 pyrgeometers (Kipp & Zonen, The Netherlands) and a CR3000 data logger (Campbell Scientific, USA). The measurement height was 6 m a.g.l.

At both systems, the measurement frequency was 20 Hz. The post-field data processing according to Mauder et al. (2013) included a raw data delay correction based on the maximization of the cross-correlation, a spike removal based on median absolute deviation, a double rotation of the wind vector and corrections for the high-frequency spectral loss (Moore, 1986), the difference between sonic temperature and air temperature (Schotanus et al., 1983) and density fluctuations (Webb et al., 1980). The calculations were done with the software package TK3.11 (Mauder and Foken, 2011). For quality assurance and quality control (QA/QC), a three-class quality flagging scheme according to Mauder et al. (2013) was applied to the 30-min turbulent statistics and fluxes. In this study, data of moderate (flag 1) and highest quality (flag 0) were used.

2.3. Doppler lidar measurements

In addition to the micrometeorological measurements, a scanning Doppler wind lidar (Streamline, HaloPhotonics Ltd., U.K.) was operated next to the meteorological tower at the forest site (Fig. 1). It emits a pulsed laser light of 1.5 μm wavelength at a pulse repetition frequency of 15 kHz and averages over 15000 pulses, i.e. its effective measurement frequency is approximately 1 Hz. The Doppler lidar determines the wind component along the optical axis, the radial velocity, from the Doppler shift of the emitted laser pulse due to the movement of atmospheric particles relative to the device. During the measurement campaign, the Doppler lidar mainly pointed vertically upward into the atmosphere to measure profiles of the vertical wind component with a vertical resolution of 30 m. Every 30 min, a velocity azimuth display scan (Browning and Wexler, 1968) with 16 points was performed in order to measure the horizontal wind profile. Data from the lowest 60 m and data with poor quality, i.e. signal-to-noise ratios <-17 dB, were discarded. For signal-to-noise rations >-17 dB, the measurement precision is better than 0.2 m s^{-1}, which was determined from the difference between lags 0 and 1 of the auto-covariance function (Lenschow and Kristensen, 1985; Frehlich, 2001). Moreover, the boundary-layer height z_i was determined from the maximum negative gradient in the backscatter intensity profile (Emeis et al., 2008).

2.4. Fourier and wavelet analysis

Fourier and wavelet analysis were performed in order to determine the mixed-layer and surface-layer velocity spectra using the 20-Hz sonic anemometer data of u, v and w, and the 1-Hz Doppler lidar data of w, where u represents the along-wind, v the crosswind, and w the vertical wind component. At first, unreliable data were removed from the time series: lidar data with low signal-to-noise ratios (Section 2.3) and sonic data that were beyond the consistency limits (Mauder et al., 2013) or that were spikes according to median absolute deviation method. Time series from which more than 5% of the data had to be rejected were excluded from the analysis. The gaps were filled by means of linear interpolation and the high-frequency sonic data were rotated into the mean wind direction, i.e. $\bar{v} = 0$.

The Fourier transform was applied to the time series data in order perform an ogive test, that was introduced by Desjardins et al. (1989) and applied to micrometeorological tower measurements by Foken et al. (1995) to test whether all low-frequency contributions are captured. This requires calculating the Fourier co-spectrum Co_{mn} of two time series m and n given as

$$\mathrm{Co}_{mn}(f) = \Re\left(F_m^*(f)\,F_n(f)\right), \tag{3}$$

where F_m and F_n are the complex coefficients of the fast Fourier transforms of m and n, f denotes the frequency, the asterisk denotes the complex conjugate and $\Re$ indicates taking the real part (Stull, 1988). The ogive function og is the cumulative integral of the co-spectrum starting from the highest frequency $f_{\max}$ (Foken et al., 2006),

$$\mathrm{og}(f_0) = \int_{f_{\max}}^{f_0} Co_{mn}(f)\,df. \tag{4}$$

If the ogive function already converges for frequencies $f_0 < 1/1800$ Hz, all turbulent motions are captured within 30 min, which was the averaging interval of the EC method.

The wavelet transform was applied to calculate the wind velocity spectra, because it resolves the time series in frequency and time domain and is also able to capture turbulent motions that do not pass by the measurement device regularly in time. The sonic data were block-averaged to 1 Hz in order to reduce the computation time. A continuous wavelet transform was applied using the Morlet mother wavelet with a frequency parameter of 6 (Torrence and Compo, 1998; Mauder et al., 2007b). The convolution of a time series m with the mother wavelet Ψ shifted by b and scaled by a gives the wavelet coefficients $W_m(a, b)$. The wavelet spectrum $S_m(a)$

Table 1
Overview of the LES configuration.

Surface heat flux ($K\,m\,s^{-1}$)	0.4 (forest); 0.16 (desert)
Roughness length (m)	2.0 (forest), 0.01 (desert)
Background wind ($m\,s^{-1}$)	0; 6
Initial boundary layer height (m)	1200
Number of grid points (–)	1200 × 1200 × 120
Domain size (m)	24000 × 24000 × 2400
Size of the forest rectangle (m)	10000 (lateral) × 6000 (longitudinal)
Time step (s)	1.8
Spatial resolution (m)	20
Simulation duration (h)	6

is obtained after squaring the wavelet coefficients and integrating over b (Hudgins et al., 1993),

$$S_m(a) = \frac{\delta j}{a} \frac{\delta t}{C_\delta} \frac{1}{N} \sum_{b=0}^{N-1} \left| W_m(a,b) \right|^2, \quad (5)$$

where $\delta j = 0.25$ is the spacing between the scales of the wavelet transform, δt is the time step of the time series, and $C_\delta = 0.776$ is a specific constant for the Morlet function (Torrence and Compo, 1998). In order to prevent edge effects, only those wavelet coefficients outside of the cone of influence were considered (Torrence and Compo, 1998). The integral over the wavelet spectrum is equal to the variance of the time series and integrating over parts of the spectrum gives the contributions of specific scales. Accordingly,

$$r_L = \frac{\sum_{a>\tau} S_m(a)}{\sum S_m(a)} \quad (6)$$

is the relative contribution of turbulent structures with time scales larger than τ.

2.5. Large-eddy simulation

The LES model PALM v3.9 (Maronga et al., 2015) was used to evaluate the influence of the desert–forest system on the boundary-layer structure under idealized conditions (Table 1). The shape of the Yatir forest was approximated by a rectangular triangle. The difference between forest and desert was encoded in different surface fluxes and roughness lengths. We did not include an additional plant canopy layer for the forest, since we are primarily interested in the boundary-layer structure and circulations above the forest and desert. Also, we only ran dry simulations, because the humidity was practically negligible during the days of the measurement campaign. Another idealization was that the simulations took place in flat terrain, although in reality the terrain around the Yatir forest consists of moderate hills and it slowly rises for 200 m from the desert measurement station to that within the forest (Section 2.1). This idealization allowed us to disentangle the influence of surface parameters on the boundary layer structure from that by the topography.

In the horizontal, periodic boundary conditions were applied. The size of the domain was sufficiently large such that the forest did not interact with its periodic copies. At the upper boundary, the vertical velocity and the perturbation pressure were zero. At the lower boundary, the standard Prandtl layer parameterization of PALM was applied, using Monin–Obukhov similarity theory within the first grid cell. The simulations were initialized with a constant potential temperature of 305 K up to 1200 m, above which there was a capping inversion of $0.01\,K\,m^{-1}$. We focused on two different cases: a simulation with zero background wind, and another with $6.0\,m\,s^{-1}$ background wind from the northwest, i.e. 315°, that is representative for the conditions during the measurement campaign. For detailed information on the LES model including the boundary conditions, sub-grid and Prandtl layer parameterization, we refer to Maronga et al. (2015).

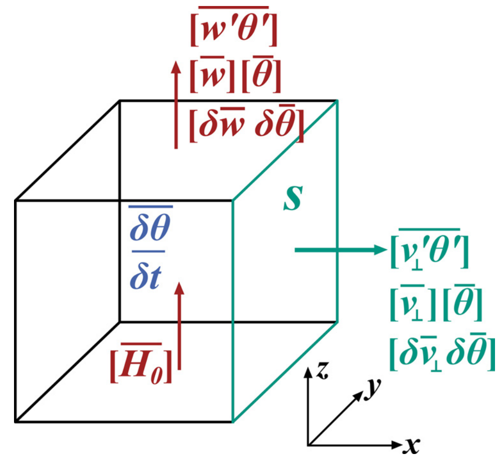

Fig. 2. Scheme describing control volume and corresponding flux components for the sensible heat flux. The flux though the lower face of the cube is the prescribed surface heat flux. Through each other face s of the cube, sensible heat is transported by the turbulent fluxes $\lfloor \overline{v'_\perp\theta'} \rfloor$, advection $\lfloor \overline{v'_\perp} \rfloor \lfloor \overline{\theta} \rfloor$ and dispersive fluxes $\left[\delta\overline{v}_\perp\delta\overline{\theta}\right]$, where $v_\perp$ is the velocity vector perpendicular to the corresponding face. For the upper face of the control volume, $v_\perp$ is replaced by w, and $\left[\overline{w'\theta'}\right]$ represents the EC flux at the top of the control volume. In addition potential temperature can be stored in the control volume over time, i.e. $\frac{\overline{\delta\theta}}{\delta t} \neq 0$. The notation is according to the text.

2.6. Control volume approach

In the LES model, the velocity vector field and the scalar fields are output at the spatial and temporal resolutions specified in Table 1. This offers the opportunity to set up a virtual cubic control volume (Fig. 2) around the measurement locations at the forest centre and in the desert and to calculate the complete flux budget equation for the sensible heat flux (Finnigan et al., 2003). Spatiotemporally averaging the equation for the potential temperature of PALM (Maronga et al., 2015) over the cubic control volume and over 30 min yields the budget equation

$$\begin{aligned} \lfloor \overline{H_0} \rfloor &= \lfloor \overline{w'\theta'} \rfloor + \sum_s \lfloor \overline{\mathbf{v'}_\perp\theta'} \rfloor_s + \lfloor \overline{w} \rfloor \lfloor \overline{\theta} \rfloor + \sum_s \lfloor \overline{\mathbf{v}}_\perp \rfloor_s \lfloor \overline{\theta} \rfloor_s \\ &+ \left[\delta\overline{w}\delta\overline{\theta}\right] + \sum_s \left[\delta_s\overline{\mathbf{v}}_\perp\delta_s\overline{\theta}\right]_s + \iiint \frac{\overline{\partial\theta}}{\partial t}\,\mathrm{d}x\mathrm{d}y\mathrm{d}z \end{aligned}, \quad (7)$$

where H_0 denotes prescribed surface heat flux, x, y and z the Cartesian coordinates, w the wind component in z direction, θ the potential temperature, $\mathbf{v}_\perp$ the velocity vector perpendicular to any lateral face s of the cube in the xz- or yz-plane. The angular brackets indicate the spatial average over the respective face of the cube, the δ corresponding spatial fluctuations, the overbars temporal averages, the primes the temporal fluctuations. The term on the left-hand side of Eq. (7) is the 'true' surface heat flux, the terms of the right-hand side denote the EC flux at the top of the control volume, the horizontal flux divergence, the vertical and horizontal advection, the vertical and horizontal dispersive fluxes (Belcher et al., 2012) and the storage of θ within the control volume. The parameterized sub-grid fluxes were added to the virtual EC flux and horizontal turbulent fluxes. For the present study, the side length of the cubic control volumes was chosen as 5 grid points and they were located at the forest centre and at the approximate location of the ceilometer in the desert.

Table 2
Daytime (5–15 UTC) surface-layer parameters at the desert site and the forest site.

Date	$u_{*,\mathrm{desert}}$ [m s^{-1}]	$u_{*,\mathrm{forest}}$ [m s^{-1}]	z/L_{desert} [–]	z/L_{forest} [–]	$\mathrm{Bo}_{\mathrm{desert}}$ [–]	$\mathrm{Bo}_{\mathrm{forest}}$ [–]	$Q_{\mathrm{B,desert}}$ [W m^{-2}]	$Q_{\mathrm{B,forest}}$ [W m^{-2}]
22 August 2013	0.26	–	−2.17	–	11.1	–	140.1	–
23 August 2013	0.24	0.78	−0.91	−0.11	8.4	12.7	158.3	409.8
24 August 2013	0.27	0.75	−0.51	−0.10	9.7	15.8	158.6	278.3
25 August 2013	0.24	0.66	−0.97	−0.18	10.0	9.4	179.1	362.1
26 August 2013	0.28	0.76	−1.25	−0.37	21.9	10.5	169.2	415.4
27 August 2013	0.26	0.81	−0.76	−0.10	8.6	7.4	179.9	418.2
28 August 2013	0.21	0.78	−2.49	−0.11	3.7	24.7	157.5	438.8
29 August 2013	0.23	0.69	−1.25	−0.21	7.3	7.1	163.1	419.1
30 August 2013	–	0.72	–	−0.70	–	15.6	–	406.0
31 August 2013	–	0.65	–	−0.26	–	17.1	–	334.8
01 September 2013	0.24	–	−1.39	–	7.0	–	207.1	–
02 September 2013	0.23	–	−1.88	–	9.5	–	161.5	–
03 September 2013	0.22	0.70	−0.98	−0.20	7.4	15.9	156.2	415.6
04 September 2013	0.25	0.76	−0.70	−0.10	6.8	11.7	159.4	343.7
05 September 2013	0.26	0.87	−0.65	−0.09	7.7	–	163.9	–
06 September 2013	0.28	0.70	−1.07	−0.23	13.3	43.5	149.5	380.7
07 September 2013	0.26	0.74	−4.00	−0.17	12.0	14.7	182.5	443.2
08 September 2013	–	0.65	–	−0.17	–	9.5	–	399.2
09 September 2013	–	0.71	–	−0.20	–	16.1	–	400.5
10 September 2013	–	0.72	–	−0.28	–	10.6	–	342.9

u_*: friction velocity; z: measurement height; L: Obukhov length; Bo: Bowen ratio; Q_B: surface buoyancy flux.

Table 3
Daytime (5–15 UTC) boundary-layer parameters.

Date	z_i [m]	U [m s^{-1}]	ϕ [°]	$w_{*,\mathrm{desert}}$ [m s^{-1}]	$w_{*,\mathrm{forest}}$ [m s^{-1}]	L_{Rau} [m]
22 August 2013	1220	6.99	296	1.78	–	3830
23 August 2013	1000	7.05	310	1.72	2.20	2700
24 August 2013	1210	8.31	286	1.76	2.05	3360
25 August 2013	1160	5.61	311	1.83	2.20	2170
26 August 2013	1030	6.25	330	1.91	2.26	2450
27 August 2013	1010	6.84	345	1.75	2.19	2290
28 August 2013	790	5.87	329	1.53	2.10	2180
29 August 2013	780	6.68	310	1.63	2.01	1930
30 August 2013	–	5.55	337	–	2.05	–
31 August 2013	–	4.77	297	–	2.01	–
01 September 2013	900	5.25	286	1.71	–	–
02 September 2013	800	5.28	303	1.64	–	–
03 September 2013	820	5.91	325	1.68	2.17	1980
04 September 2013	930	6.67	285	1.68	1.96	2580
05 Sept 2013	–	6.74	312	1.70	2.43	–
09 Sept 2013	980	5.49	316	–	2.13	–
10 Sept 2013	1420	6.19	348	–	2.20	–

z_i: boundary-layer height above the forest, U: mean wind speed at 200–500 m a.g.l., ϕ: mean wind direction at 200–500 m a.g.l., w_*: convective velocity scale, L_{Rau}: convective length scale according to Raupach and Finnigan (1995).

3. Results and discussion

3.1. Surface turbulent heat fluxes and energy balance closure

The average daily cycles of net radiation and surface turbulent heat fluxes at both sites (Fig. 3) illustrate the extremely dry conditions in the area with a mean daytime Bowen-ratio of 8.4 at the desert site and 12.5 at the forest site. The results are in accordance with long-term measurements of Rotenberg and Yakir (2011) at the Yatir forest, who found Bowen-ratios larger than 10 and sensible heat fluxes up to 926 W m^{-2} during summer. Fig. 3 also shows the increased sensible heat flux above the forest, for which several explanations can be found:

i) Due to its low albedo (12.5%) as compared to the desert (33.7%), the forest reflects less shortwave radiation, e.g. about 200 W m^{-2} less around noontime. In addition, the long-wave upwelling radiation at the forest is lower by about 100 W m^{-2}. This surplus of energy is mainly put into Q_H because of the extremely dry conditions.
ii) The high surface roughness length of the forest increases friction, which leads to an increased turbulence intensity above the forest site. As a result, the friction velocity at the forest site is about 3 times larger than at the desert site (Table 2). This increased turbulence intensity above the forest facilitates the vertical transfer of heat (Juang et al., 2007) which is known as the canopy convector effect (Rotenberg and Yakir, 2010, 2011).

Regarding the surface energy balance, Q_G was not measured, although it probably has a large amplitude, especially at the desert site (Heusinkveld et al., 2004). However, on a daily basis, and especially over a longer period, Q_G should be zero on average, because the energy that is stored in the soil during the day is released during the evening and the night. Leuning et al. (2012) confirmed that the ratios of $(Q_H + Q_E)/(-Q_S{}^*)$ and $(Q_H + Q_E)/(-Q_S{}^* - Q_G)$ on a daily time scale are equivalent. Accordingly, the average energy balance

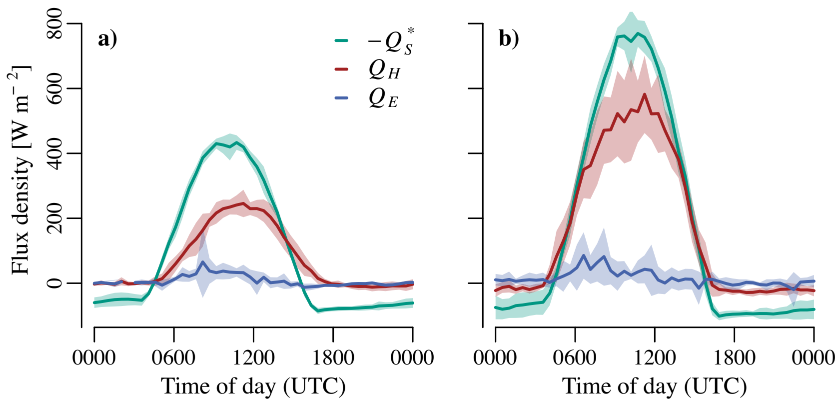

Fig. 3. Average net radiation $-Q_S^*$, sensible heat flux Q_H and latent heat flux Q_E at (a) the desert site and (b) the forest site between 22 August and 11 September 2013. The shaded areas indicate the standard deviation.

closure at both sites was calculated by integrating $-Q_S$*, Q_H and Q_E over the whole measurement campaign, and the energy balance was found to be not closed at the desert site ($R = 0.81$) whilst it was closed at the forest site ($R = 1.00$). Under the assumption that under these extremely dry conditions only Q_H and not Q_E is considerably underestimated, we could correct for this systematic error at the desert site by adding the complete 'missing' energy (0.19 Q_S*) to Q_H. This would increase the sensible heat flux above the desert by 20%.

Consequently, there is a difference in surface buoyancy Q_B (Eq. (2), Table 2) between forest and desert of about 270–340 W m^{-2} during daytime, or of about 220–290 W m^{-2} if we account for the underestimation of Q_H at the desert site. If the forest is large enough (Section 3.2), this might induce a secondary circulation (Section 3.3) that could affect in turn the measurements of the turbulent heat fluxes (Section 3.4).

3.2. Boundary-layer convective scaling

For generating secondary circulations, surface patches must be large enough to induce advection at the boundary-layer scale. In the convective boundary-layer, large eddies exchange air between the surface and boundary-layer top within a time scale of z_i/w_*, which is usually a few tens of minutes. Accordingly, the surface heterogeneity should be larger than the distance L_{Rau} that the flow travels during this mixing time scale (Raupach and Finnigan, 1995),

$$L_{\mathrm{Rau}} = C_{\mathrm{Rau}} \frac{U z_i}{w*}, \tag{8}$$

where U is the mean wind speed of the well-mixed bulk of the convective boundary layer, which was determined from the wind profile of the Doppler lidar between 200 m and 500 m a.g.l. (Table 3), and $C_{\mathrm{Rau}} = 0.8$ (Mahrt, 2000) is a non-dimensional coefficient. The blending height concept (Mahrt, 2000) is an alternative method for estimating the minimum size of surface heterogeneities. However, this approach was not applicable for the convective boundary layer at the Yatir site, since it only considers vertical mixing due to shear-induced turbulence.

L_{Rau} was calculated using the daytime averages of U, z_i and w_* (Table 3). For most measurement days, it was found that the size of surface heterogeneities should be at least around 2–2.5 km. On 22 August and 24 August, L_{Rau} was >3 km due to the relatively deep boundary layers on 22 August and 24 August and the relatively high wind speed on 24 August. The shape of the Yatir forest is approximately a triangle, with a size of 10 km in East–West direction and 6 km in North–South direction. Accordingly, it should be always large enough to generate secondary circulations. Furthermore, since the mean daytime boundary-layer height above the forest was about 800–1400 m (Table 3) with maximum values of about 2000 m around noontime, the forest also fulfils the prerequisites by Patton et al. (2005) who found that heterogeneities with a size of around 4–9 times the boundary-layer height are most effective in generating secondary circulations. Recently, van Heerwaarden et al. (2014) stressed that the optimum ratio of heterogeneity size to boundary-layer height increases with increasing heat flux amplitude.

3.3. Secondary circulation above the forest

The surface buoyancy flux above Yatir forest is ~220–290 W m^{-2} larger than in the desert (Section 3.1) and that the forest is large enough to cause boundary-layer scale advection (Section 3.2). Accordingly, a secondary circulation might develop in that area, which was tested by means of LES and analyzing the wind measurements of the Doppler lidar and the sonic anemometers.

As described in Section 2.5, two different LES runs were performed, one with zero background wind and one with a background wind of 6 m s^{-1} from 315° that is representative of the typical meteorological conditions during the measurement campaign (Table 3). The boundary-layer height was initialized with 1200 m (Section 2.5) and grew up to about 1500 m after 3 h of simulation. Thus, ratio of heterogeneity scale to boundary-layer height was about 5–7. The forest was encoded as an isolated patch with a larger surface heat flux that covered about 5% of the model domain and exhibited a 2.3 times higher surface buoyancy flux than the domain average that is almost equal to the desert buoyancy flux. For such heat-flux amplitudes, van Heerwaarden et al. (2014) confirmed the suggested ideal ratio of heterogeneity scale to boundary-layer height by Patton et al. (2005) of 4–9. For the zero-wind case (Fig. 4a,c), a strong updraft above the forest was found after 3 h of simulation with vertical wind speeds >3 m s^{-1} at the forest centre. The desert area showed hexagonal patterns that are typical for open cell convection (Schmidt and Schumann, 1989; Träumner et al., 2014). However, it seems that updrafts >2 m s^{-1} were suppressed within a distance of <5 km from the forest border (Fig. 4c). Accordingly, at low wind speeds, the forest is able to induce meso-scale circulations similar to those which were detected with aircrafts above lakes in the boreal forest (Sun et al., 1997), above patches with different surface moisture in the Sahel region (Taylor et al., 2007; Garcia-Carreras et al., 2010) and the Great Plains, USA (Kang et al., 2007), or above irrigated agricultural land in arid regions (Mahrt et al., 1994; Wulfmeyer et al., 2014).

For the LES run with background wind (Fig. 4b,d), only a weak net updraft was found above the forest (Fig. 4b). The whole simulation domain was dominated by bands of up- and downdrafts

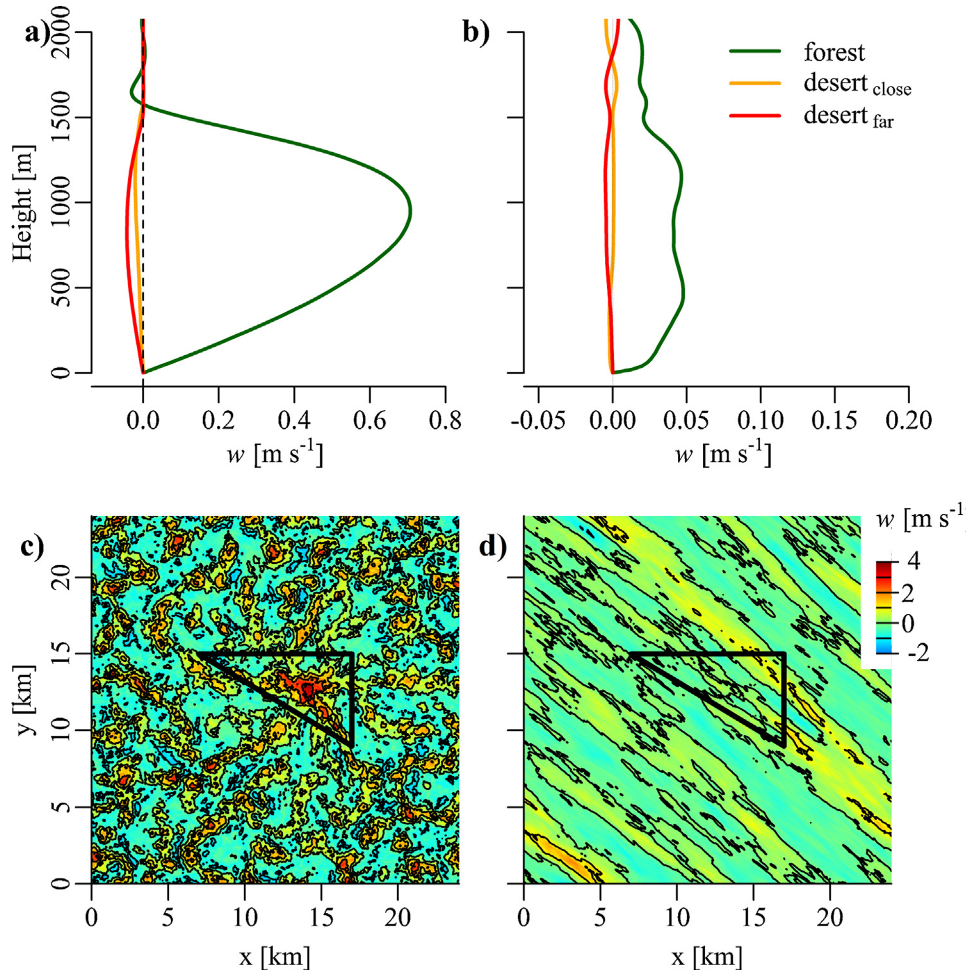

Fig. 4. The vertical wind component w from the LES runs without (a,c) and with geostrophic wind (b,d) after 3 h of simulation; panels (a) and (b) show the spatially-averaged profiles above the forest, above those parts of the desert that are within a distance of 10 km from the forest centre (desert$_{close}$) and above those parts of the desert further away from the forest (desert$_{far}$); panels (c) and (d) show an horizontal cross-section of 30-min averages of w at a height of approximately 0.6 z_i; the tick black lines in (c) and (d) show the location of the forest, i.e. the area with the increased surface heat flux.

with absolute vertical wind speeds mostly <1 m s^{-1} (Fig. 4d) that could be traces of horizontal roll convection (Etling and Brown, 1993). There were slightly stronger updrafts ($\bar{w}$ > 1 m s^{-1}) downwind of the forest, but all in all, the large-eddy-simulation did not provide clear evidence for a strong stationary secondary circulation between forest and desert under these wind conditions. This is in accordance with aircraft measurements of Dixon et al. (2013), who found that heterogeneity-induced circulations only existed up to background wind speeds of about 5 m s^{-1} (Dixon et al., 2013), and a LES study of Kang and Lenschow (2014), where background wind inhibited the formation of a heterogeneity-induced secondary circulation.

Then, the vertical wind velocity profiles above the forest measured with the Doppler lidar were analyzed in order to test whether they confirm the findings from the LES. According to the modelling results, the secondary circulation should be visible as a persistent vertical updraft above the forest. A persistent updraft was considered as (i) a mean vertical wind velocity >0.5 m s^{-1} for (ii) at least a 3-h period and (iii) extending >500 m in height. Persistent updrafts were found on 5 days during the measurement campaign (22 August, 30 August, 31 August, 1 September, 10 September) above the forest, although the mean horizontal wind speed (U) was relatively high (4.8–7.0 m s^{-1}) on those days (Table 3). An example of a strong persistent updraft on 10 September is shown in Fig. 5a. Interestingly, relatively low wind speeds (<3 m s^{-1}) and low friction velocities (<0.5 m s^{-1}) were measured at the forest tower during that event (Fig. 5b,c), which presumably allowed the development of a well-shaped secondary circulation. However, all these events occurred before 12 h UTC, i.e. before the onset of the sea breeze (Section 2.1) that usually arrives at the measurement site during the early afternoon hours. The sea breeze circulation is associated with higher wind speeds. The development of a distinct secondary circulation is weakened and the persistent updraft moves downwind of the forest (Fig. 4d).

In addition, it was tested whether such a secondary circulation becomes apparent as significant low-frequency contributions at atmospheric wind spectra. For this reason, wavelet spectra (Section 2.4) from the sonic anemometer data and the w time series of the vertically pointing Doppler lidar were investigated for time scales >30 min. Here, we show examples from 25 August and from 27 August. We found low-frequency contributions to the w spectra in the entire mixed layer (Fig. 6a,d) and especially in the u and v spectra above the desert site (Fig. 6b,e). These low-frequency contributions could be either caused by a stationary secondary circulation between forest and desert that do not obey mixed-layer scaling (Kang, 2009), or by buoyancy-driven convective coherent structures that obey mixed-layer scaling (Kaimal et al., 1976; Kaimal, 1978; Højstrup, 1981; McNaughton, 2004). The measured spectra were also compared with the spectral model of Højstrup (1981) that explicitly considers the low-frequency contributions

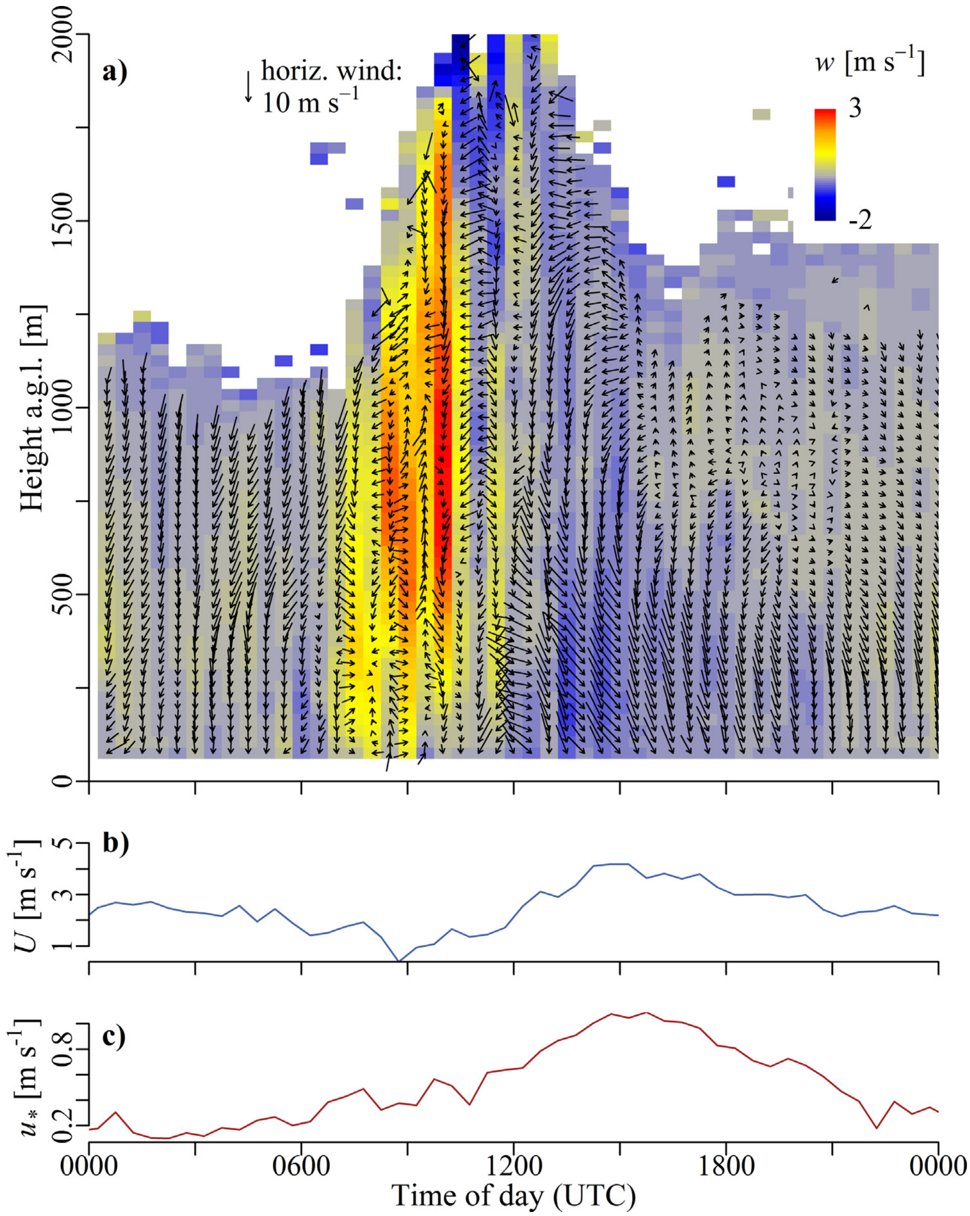

Fig. 5. Doppler lidar measurements of the wind field above the Yatir forest on 10 September 2013 (a); the arrows show the horizontal wind speed and wind direction, the colours indicate 30-min averages of the vertical wind component w; panels (b) and (c) show the horizontal wind speed U and the friction velocity u_* measured with the sonic anemometer above the forest canopy.

of convective coherent structures to the surface-layer horizontal wind components. The data from the forest site show a good agreement with the model of Højstrup (1981), but the measured low-frequency contributions at the desert site were larger than predicted by the model, especially on 25 August. These additional contributions may originate from secondary circulations induced by the forest-desert heterogeneity, even though the Doppler lidar did not show a mean vertical updraft above the forest on those days. Above the forest, the u and v spectra were shifted to higher frequencies, because in the roughness sublayer the convective coherent structures were less dominant and probably broken up into smaller organized structures (Raupach et al., 1996; Finnigan, 2000). Accordingly, the spectral ratios r_L (Eq. (6)) of the u and v spectra above the forest are significantly smaller than above the desert (Table 4). The

Table 4
Mean values of low-frequency contribution (time scales > 30 min) r_L to spectra of wind components above desert and forest for the whole measurement campaign.

Wind component	Instrument	Height a.g.l.	r_L (desert)	r_L (forest)
u	R3-50 sonic anemometer	6(19)[a] m	0.31 ± 0.08	0.11 ± 0.04
v	R3-50 sonic anemometer	6(19)[a] m	0.29 ± 0.07	0.12 ± 0.03
w	R3-50 sonic anemometer	6(19)[a] m	0.02 ± 0.01	0.01 ± 0.003
w	Streamline lidar	100 m	–	0.11 ± 0.07
w	Streamline lidar	400 m	–	0.13 ± 0.04
w	Streamline lidar	800 m	–	0.16 ± 0.08

[a] Measurement height of sonic anemometers was 6 m at the desert site and 19 m at the forest site.

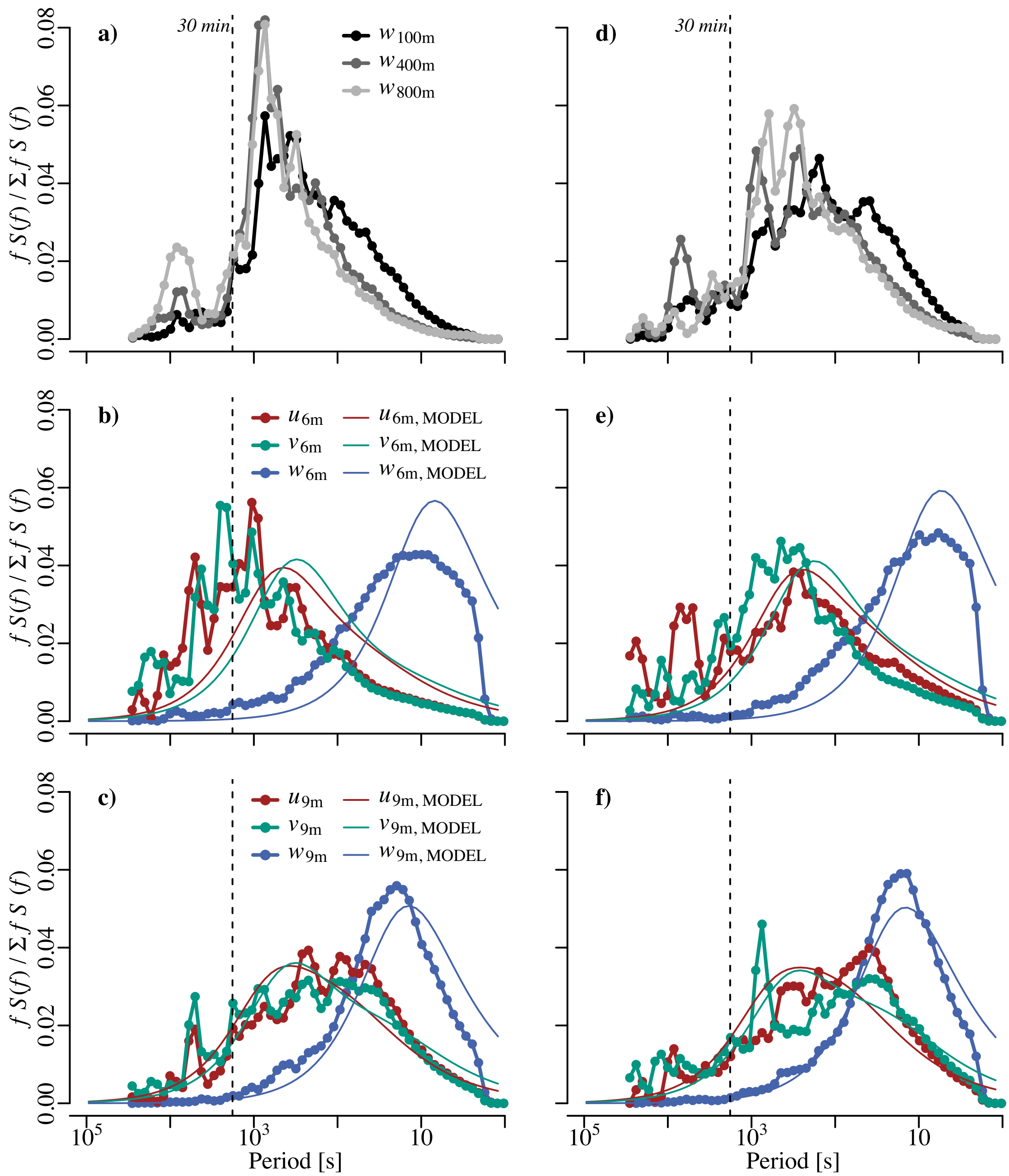

Fig. 6. Normalized wavelet spectra of the three wind components u, v and w using the data from (a to c) 25 August and (d to f) 27 August 2014. The mixed-layer w spectra (a,d) were determined from the Streamline data, the surface-layer spectra above (d,e) the desert and (c,f) the forest from the sonic anemometer measurements. The surface-layer spectra were compared with the spectral model of Højstrup (1981). The vertical dashed line indicates a period of 30 min which was the averaging time for the EC measurements.

w spectra from the surface layer did not show any significant low-frequency contribution (Table 3, Fig. 6) which is in accordance with the spectral model. To sum up, we found significant low-frequency contributions, especially in the surface-layer u and v spectra that are most likely caused by convective coherent structures, and, to a lesser extent, also by a stationary secondary circulation between the forest and the desert.

3.4. Implications for flux measurements and energy balance closure

As presented in the previous section, convective coherent structures and secondary circulations induce low-frequency contributions to the surface-layer horizontal wind spectra with time scales larger than the averaging time of the EC systems. The low-frequency contributions above the desert site were larger than above the forest site at the respective measurement levels of the EC systems (Table 4). Hence, the energy balance at the desert site was not closed, while it was closed at the forest site (Section 3.1).

This relation suggests that the averaging time of 30 min is not sufficient to capture all atmospheric motions contributing to surface-atmosphere exchange. In order to verify this assumption, ogive functions for the desert site and the forest site were calculated (Section 2.4). Here, the ogives were calculated using the daytime measurements between 7 and 15 UTC for the momentum

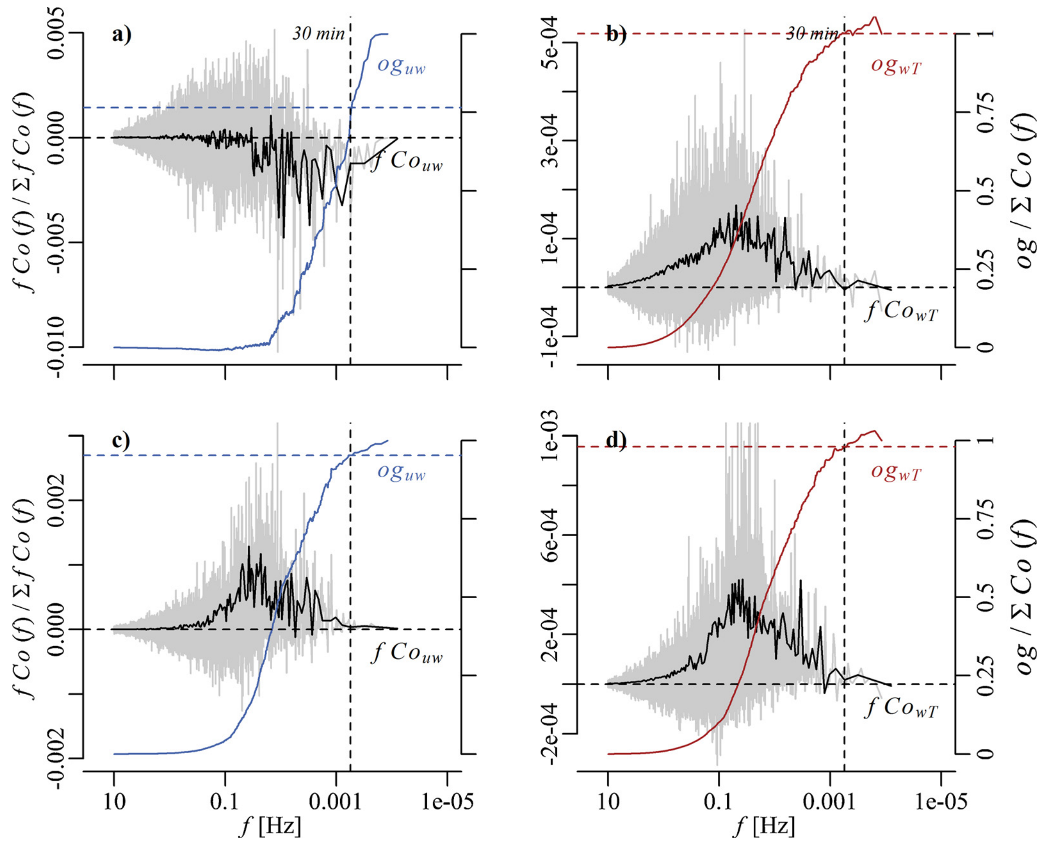

Fig. 7. Fourier co-spectra and ogive functions normalized by the co-spectrum for momentum flux (a,c) and sensible heat flux (b,d) at the desert site (a,b) and the forest site (c,d) on 25 August 2013. For this analysis only periods up to 3 h were considered. The grey line indicates the original co-spectrum, the black line the smoothed co-spectrum, the solid coloured lines the normalized ogive function, and the horizontal dashed line the respective value of the ogive function at a period of 30 min.

flux following Foken et al. (2006) and for the sensible heat flux, by considering all frequencies up to a period of 3 h. Fig. 7 shows examples of co-spectra and ogive functions for 25 August, and these results are representative for the whole measurement campaign. For the momentum flux at the desert site, the ogive function was not convergent within 30 min, but it was convergent at the forest site. For the sensible heat flux, both ogives were convergent within 30 min. Thus, the ogive test does not indicate any significant low-frequency contribution to the sensible heat flux. However, this is not surprising since the surface-layer w spectra did not show any low-frequency contributions (Section 3.3, Fig. 6). In the surface layer, the horizontal wind components are affected by the secondary circulation and the convective coherent structures. For this reason, the ogive function of the momentum flux at the desert site does not converge and we expect that the horizontal sensible heat fluxes $\overline{u'T'}$ and $\overline{v'T'}$ are similarly affected by the secondary circulations. In other words, we expect that the low-frequency circulations at the desert site cause advection and horizontal flux divergence (Finnigan et al., 2003; Foken et al., 2010, 2011), but the calculation of the co-spectra of u and T and of v and T did not provide any meaningful result. Moreover, a stationary secondary circulation between the forest and the desert with a lifetime >3 h could not be captured with this approach that is based on a point measurement.

Our results are different from the results of Heusinkveld et al. (2004) from measurements in the nearby Negev desert. They did not find any significant low-frequency contributions to the fluxes and they were able to close the energy balance. However, Heusinkveld et al. (2004) conducted their measurements further inside the desert, and far away from any pronounced surface heterogeneity like the Yatir forest. Thus, at their site, secondary circulations were probably not relevant. No significant low-frequency contributions affected the surface-layer measurements and consequently, the energy balance was closed.

Furthermore, LES offers the possibility to calculate the complete flux budget (Finnigan et al., 2003), following the control volume approach presented in Section 2.6. This was done for one control volume above the desert site (Fig. 8a) and one above the forest site (Fig. 8b) using the model run with a background wind of 6 m s^{-1}. The LES reproduces that, above the forest, the sensible heat flux estimate using the EC method is identical to the surface sensible heat flux, i.e. the turbulent fluxes are not underestimated and the energy balance should be closed. At the desert site, the virtual EC flux underestimates the surface sensible heat flux by 30%. This underestimation at the desert site is due to net advection of sensible heat out of the control volume. The forest site is also subject to a net advection of sensible heat into its control volume, but this is compensated by the horizontal flux divergence. However, it should be noted that no canopy layer and thus to roughness sublayer was represented in the LES model and the top of the control volumes was at 100 m a.g.l. due to the coarse grid resolution. Nevertheless, this approach successfully reproduces that the EC method tends to systematically underestimate the surface heat fluxes at the desert site, but not at the forest site, and that advection is a major reason. This advection is caused by turbulent structures with timescales larger than 30 min that become apparent as low-frequency contributions to the horizontal wind spectra in the surface layer (Fig. 6) and to the surface-layer momentum flux (Fig. 7).

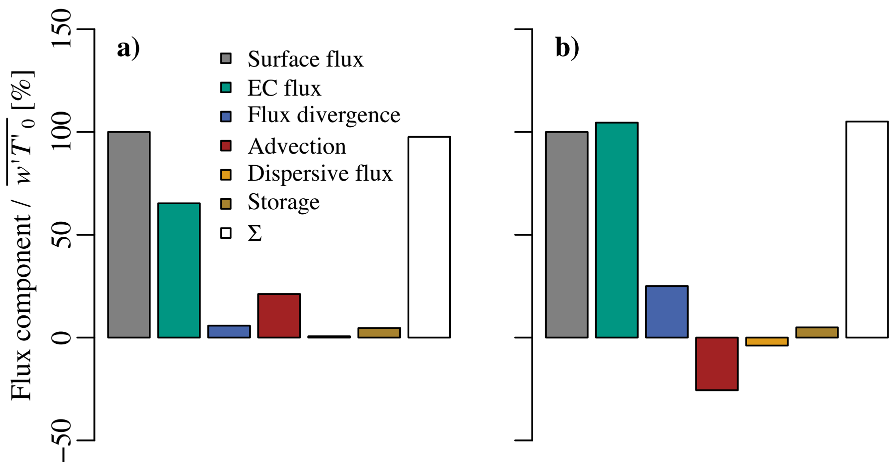

Fig. 8. Components of the sensible heat flux budget normalized by the prescribed surface flux determined from the LES control volume method for the desert site (a) and the forest site (b) for a background wind of 6 m s^{-1}; the Σ indicates the sum of the EC flux, flux divergence, advection, dispersive flux and storage components.

4. Conclusions

Due to its isolated location, the Yatir forest represents a pronounced surface heterogeneity that is an ideal natural laboratory for investigating secondary circulations and its affect on micrometeorological measurements under constant fair weather conditions. Because of its low albedo and its increased surface roughness, the forest creates higher turbulent heat fluxes which results in horizontal surface buoyancy flux differences of 220–290 W m^{-2}. Moreover, the forest has dimensions of about 5 times the usual boundary-layer height, which is ideal for inducing a strong secondary circulation (Patton et al., 2005). Moreover, it is larger than the convective length scale of Raupach and Finnigan (1995) and is thus able to modify the complete overlying atmospheric boundary layer.

The LES run without background wind confirmed the development of a secondary circulation that becomes apparent as a strong persistent updraft above the forest. However, in the Doppler lidar measurements, such persistent vertical updrafts were only found on 5 of 16 measurements days, during hours with relatively low wind speeds. The LES confirmed that, with a common background flow of 6 m s^{-1}, the vertical velocity field is dominated by convective coherent structures that are not related to the surface heterogeneity. The weak updraft downwind of the forest could not be captured with a single Doppler lidar located at the forest centre.

Secondary circulations and convective coherent structures are responsible for the underestimation of the turbulent fluxes by 19% at the desert site. The associated low-frequency contributions with timescales >30 min cannot be captured with the standard EC method. The ogive test indicated low-frequency contributions to co-spectrum of u and w, but not to the co-spectrum w and T. Our data suggest that the 'missing' energy is mainly contained in advection and the horizontal fluxes and not in the low frequencies of the vertical turbulent fluxes. Analyzing the complete flux budget of a virtual control volume in the LES model confirmed that the low-frequency structures cause considerable advection at the desert site that is responsible for the non-closure of the energy balance. Above the forest, the surface-layer spectra are shifted to higher frequencies, all ogive functions converge within 30 min, and the energy balance is closed, presumably because the large eddies are broken up into smaller structures in the roughness sublayer of the forest.

Thus, it could be shown that differences in landuse do not only have a strong effect on the local energy budget, but also affect the structure of the overlying boundary layer. The afforestation efforts in the Yatir area probably also modify the local boundary-layer height, the cloud formation and the regional weather and climate. Furthermore, secondary circulations are not restricted to special sites like the Yatir forest. Such effects could occur in every landscape that is characterized by sufficiently large surface patches that have different surface buoyancy fluxes, e.g. due to differences in surface moisture, different agricultural crops or in urban areas. For investigating the effects of landuse on boundary-layer properties, a careful selection of the measurement location is required. We recommend performing a simple numerical simulation in advance of the campaign for this purpose. Moreover, an integrated approach using surface flux measurements, ground-based remote sensing measurements and numerical simulation gives the best insights into the processes at work.

Acknowledgements

The authors would like to thank the staff from the Department of Earth and Planetary Sciences of the Weizmann Institute of Science for the assistance during the field campaign. This work was conducted within the Helmholtz Young Investigator Group "Capturing all relevant scales of biosphere-atmosphere exchange – the enigmatic energy balance closure problem", which is funded by the Helmholtz-Association through the President's Initiative and Networking Fund, and by KIT.

References

Baldocchi, D.D., 2003. Assessing the eddy covariance technique for evaluating carbon dioxide exchange rates of ecosystems: past, present and future. Glob. Change Biol. 9, 479–492.
Belcher, S.E., Harman, I.N., Finnigan, J.J., 2012. The wind in the willows: flows in forest canopies in complex terrain. Annu. Rev. Fluid Mech. 44, 479–504.
Bradshaw, P., 1967. 'Inactive' motion and pressure fluctuations in turbulent boundary layers. J. Fluid Mech. 30, 241–258.
Browning, K.A., Wexler, R., 1968. The determination of kinematic properties of a wind field using Doppler radar. J. Appl. Meteorol. 7, 105–113.
Caughey, S.J., Palmer, S.G., 1979. Some aspects of turbulence structure through the depth of the convective boundary layer. Q.J.R. Meteorol. Soc. 105, 811–827.
Charuchittipan, D., Babel, W., Mauder, M., Leps, J.P., Foken, T., 2014. Extension of the averaging time in eddy-covariance measurements and its effect on the energy balance closure. Bound. Layer Meteorol. 152, 303–327.
Courault, D., Drobinski, P., Brunet, Y., Lacarrere, P., Talbot, C., 2007. Impact of surface heterogeneity on a buoyancy-driven convective boundary layer in light winds. Bound. Layer Meteorol. 124, 383–403.
Dalu, G.A., Pielke, R.A., 1993. Vertical heat fluxes generated by mesoscale atmospheric flow induced by thermal inhomogeneities in the PBL. J. Atmos. Sci. 50, 919–926.
Dayan, U., Shenhav, R., Graber, M., 1988. The spatial and temporal behavior of the mixed layer in Israel. J. Appl. Meteorol. 27, 1382–1394.
Dayan, U., Rodnizki, J., 1999. The temporal behavior of the atmospheric boundary layer in Israel. J. Appl. Meteorol. 38, 830–836.

Desjardins, R.L., MacPherson, J.I., Schuepp, P.H., Karanja, F., 1989. An evaluation of aircraft flux measurements of CO_2, water vapor and sensible heat. Bound. Layer Meteorol. 47, 55–69.
Dixon, N.S., Parker, D.J., Taylor, C.M., Garcia-Carreras, L., Harris, P.P., Marsham, J.H., Polcher, J., Woolley, A., 2013. The effect of background wind on mesoscale circulations above variable soil moisture in the Sahel. Q.J.R. Meteorol. Soc. 139, 1009–1024.
Driedonks, A.G.M., Tennekes, H., 1984. Entrainment effects in the well-mixed atmospheric boundary layer. Bound. Layer Meteorol. 30, 75–105.
Drobinski, P., Brown, R., Flamant, P., Pelon, J., 1998. Evidence of organized large eddies by ground-based Doppler lidar, sonic anemometer and sodar. Bound. Layer Meteorol. 88, 343–361.
Emeis, S., Schäfer, K., Münkel, C., 2008. Surface-based remote sensing of the mixing-layer height – a review. Meteorol. Z. 17, 621–630.
Etling, D., Brown, R.A., 1993. Roll vortices in the planetary boundary layer: a review. Bound. Layer Meteorol. 65, 215–248.
Finnigan, J.J., Clement, R., Malhi, Y., Leuning, R., Cleugh, H.A., 2003. A re-evaluation of long-term flux measurement techniques part I: averaging and coordinate rotation. Bound. Layer Meteorol. 107, 1–48.
Finnigan, J., 2000. Turbulence in plant canopies. Annu. Rev. Fluid Mech. 32, 519–571.
Foken, T., Dlugi, R., Kramm, G., 1995. On the determination of dry deposition and emission of gaseous compounds at the biosphere–atmosphere interface. Meteorol. Z. 4, 91–118.
Foken, T., Wimmer, F., Mauder, M., Thomas, C., Liebethal, C., 2006. Some aspects of the energy balance closure problem. Atmos. Chem. Phys. 6, 4395–4402.
Foken, T., 2008. The energy balance closure problem: an overview. Ecol. Appl. 18, 1351–1367.
Foken, T., Aubinet, M., Finnigan, J.J., Leclerc, M.Y., Mauder, M., Paw, U.K.T., 2011. Results of a panel discussion about the energy balance closure correction for trace gases. Bull. Am. Meteorol. Soc. 92, ES13–ES18.
Foken, T., Mauder, M., Liebethal, C., Wimmer, F., Beyrich, F., Leps, J.P., Raasch, S., DeBruin, H., Meijninger, W., Bange, J., 2010. Energy balance closure for the LITFASS-2003 experiment. Theor. Appl. Climatol. 101, 149–160.
Frehlich, R., 2001. Estimation of velocity error for Doppler lidar measurements. J. Atmos. Oceanic Technol. 18, 1628–1639.
Garcia-Carreras, L., Parker, D.J., Taylor, C.M., Reeves, C.E., Murphy, J.G., 2010. Impact of mesoscale vegetation heterogeneities on the dynamical and thermodynamic properties of the planetary boundary layer. J. Geophys. Res. Atmos. 115, D03102.
Garratt, J.R., 1990. The internal boundary layer – a review. Bound. -Layer Meteorol. 50, 171–203.
Grünzweig, J.M., Lin, T., Rotenberg, E., Schwartz, A., Yakir, D., 2003. Carbon sequestration in arid-land forest. Glob. Change Biol. 9, 791–799.
Hendricks-Franssen, H.J., Stöckli, R., Lehner, I., Rotenberg, E., Seneviratne, S.I., 2010. Energy balance closure of eddy-covariance data: a multisite analysis for European FLUXNET stations. Agric. For. Meteorol. 150, 1553–1567.
Heusinkveld, B.G., Jacobs, A.F.G., Holtslag, A.A.M., Berkowicz, S.M., 2004. Surface energy balance closure in an arid region: role of soil heat flux. Agric. For. Meteorol. 122, 21–37.
Higgins, C.W., Pardyiak, E., Froidevaux, M., Simeonov, V., Parlange, M.B., 2013. Measured and estimated water vapor advection in the atmospheric surface layer. J. Hydrometeorol. 14, 1966–1972.
Hiyama, T., Strunin, M.A., Tanaka, H., Ohta, T., 2007. The development of local circulations around the lena river and their effect on tower-observed energy imbalance. Hydrol. Process. 21, 2038–2048.
Højstrup, J., 1981. A simple model for the adjustment of velocity spectra in unstable conditions downstream of an abrupt change in roughness and heat flux. Bound. Layer Meteorol. 21, 341–356.
Hudgins, L.E., Mayer, M.E., Friehe, C.A., 1993. Fourier and wavelet analysis of atmospheric turbulence. In: Meyers, E., Roques, S. (Eds.), Progress in Wavelet Analysis and Applications. Editions Frontiers, Gif-sur-Yvette, France, pp. 491–498.
Juang, J.Y., Katul, G., Siqueira, M., Stoy, P., Novick, K., 2007. Separating the effects of albedo from eco-physiological changes on surface temperature along a successional chronosequence in the southeastern United States. Geophys. Res. Lett. 34, L21408.
Kaimal, J.C., 1978. Horizontal velocity spectra in an unstable surface layer. J. Atmos. Sci. 35, 18–24.
Kaimal, J.C., Wyngaard, J.C., Haugen, D.A., Coté, O.R., Izumi, Y., Caughey, S.J., Readings, C.J., 1976. Turbulence structure in the convective boundary layer. J. Atmos. Sci. 33, 2152–2169.
Kang, S.L., Lenschow, D.H., 2014. Temporal evolution of low-level winds induced by two-dimensional mesoscale surface heat-flux heterogeneity. Bound. Layer Meteorol. 151, 501–529.
Kang, S.-L., 2009. Temporal oscillations in the convective boundary layer forced by mesoscale surface heat-flux variations. Bound. Layer Meteorol. 132, 59–81.
Kang, S.-L., Davis, K.J., LeMone, M., 2007. Observations of the ABL structures over a heterogeneous land surface during IHOP_2002. J. Hydrometeorol. 8, 221–244.
Kropfli, R.A., Hildebrand, P.H., 1980. Three-dimensional wind measurements in the optically clear planetary boundary layer with dual-Doppler radar. Radio Sci. 15, 283–296.
Lee, X., Black, T.A., 1993. Atmospheric turbulence within and above a douglas-fir stand. Part II: eddy fluxes of sensible heat and water vapour. Bound. Layer Meteorol. 64, 369–389.
Lenschow, D.H., Kristensen, L., 1985. Uncorrelated noise in turbulence measurements. J. Atmos. Oceanic Technol. 2, 68–81.
Leuning, R., van Gorsel, E., Massman, W.J., Isaac, P.R., 2012. Reflections on the surface energy imbalance problem. Agric. For. Meteorol. 156, 65–74.
Levi, Y., Shilo, E., Setter, I., 2011. Climatology of a summer coastal boundary layer with 1290-MHz wind profiler radar and a WRF simulation. J. Appl. Meteorol. Climatol. 50, 1815–1826.
Liu, G., Sun, J., Yin, L., 2011. Turbulence characteristics of the shear-free convective boundary layer driven by heterogeneous surface heating. Bound. Layer Meteorol. 140, 57–71.
Mahfouf, J.F., Richard, E., Mascart, P., 1987. The influence of soil and vegetation on the development of mesoscale circulations. J. Clim. Appl. Meteorol. 26, 1483–1495.
Mahrt, L., 1998. Flux sampling errors for aircraft and towers. J. Atmos. Oceanic Technol. 15, 416–429.
Mahrt, L., 2000. Surface heterogeneity and vertical structure of the boundary layer. Bound. Layer Meteorol. 96, 33–62.
Mahrt, L., Sun, J., Vickers, D., MacPherson, J.I., Pederson, J.R., Desjardins, R.L., 1994. Observations of fluxes and inland breezes over a heterogeneous surface. J. Atmos. Sci. 51, 2484–2499.
Maronga, B., Gryschka, M., Heinze, R., Hoffmann, F., Kanani-Sühring, F., Keck, M., Ketelsen, K., Letzel, M.O., Sühring, M., Raasch, S., 2015. The parallelized large-eddy simulation model (PALM) version 4.0 for atmospheric and oceanic flows: model formulation recent developments, and future perspectives. Geosci. Model Dev. Discuss. 8, 1539–1637.
Maronga, B., Raasch, S., 2013. Large-eddy simulations of surface heterogeneity effects on the convective boundary layer during the LIFASS-2003 experiment. Bound. Layer Meteorol. 146, 17–44.
Mauder, M., Jegede, O.O., Okogbue, E.C., Wimmer, F., Foken, T., 2007a. Surface energy balance measurements at a tropical site in West Africa during the transition from dry to wet season. Theor. Appl. Climatol. 89, 171–183.
Mauder, M., Desjardins, R.L., MacPherson, I., 2007b. Scale analysis of airborne flux measurements over heterogeneous terrain in a boreal ecosystem. J. Geophys. Res. 112, D13112.
Mauder, M., Cuntz, M., Drüe, C., Graf, A., Rebmann, C., Schmid, H.P., Schmidt, M., Steinbrecher, R., 2013. A strategy for quality and uncertainty assessment of long-term eddy-covariance measurements. Agric. For. Meteorol. 169, 122–135.
Mauder, M., Foken, T., 2011. Documentation and Instruction Manual of the Eddy-Covariance Software Package TK3. University of Bayreuth, Department of Micrometeorology, Arbeitsergebnisse 46, Bayreuth, Germany.
McNaughton, K.G., 2004. Turbulence structure of the unstable atmospheric surface layer and transition to the outer layer. Bound. Layer Meteorol. 112, 199–221.
Moore, C.J., 1986. Frequency response corrections for eddy correlation systems. Bound. Layer Meteorol. 37, 17–35.
Panin, G.N., Bernhofer, Ch., 2008. Parametrization of turbulent fluxes over inhomogeneous landscapes. Izv. Atmos. Oceanic Phys. 44, 701–716.
Patton, E.G., Sullivan, P.P., Moeng, C.H., 2005. The influence of idealized heterogeneity on wet and dry planetary boundary layers coupled to the land surface. J. Atmos. Sci. 62, 2078–2097.
Raupach, M.R., Finnigan, J.J., 1995. Scale issues in boundary-layer meteorology: surface energy balances in heterogeneous terrain. Hydrol. Process. 9, 589–612.
Raupach, M.R., Finnigan, J.J., Brunet, Y., 1996. Coherent eddies and turbulence in vegetation canopies: the mixing-layer analogy. Bound. Layer Meteorol. 78, 351–382.
Rotenberg, E., Yakir, D., 2010. Contribution of semi-arid forests to the climate system. Science 327, 451–454.
Rotenberg, E., Yakir, D., 2011. Distinct patterns of changes in surface energy budget associated with forestation in the semiarid region. Glob. Change Biol. 17, 1536–1548.
Sakai, R.K., Fitzjarrald, D.R., Moore, K.E., 2001. Importance of low-frequency contributions to eddy fluxes observed over rough surfaces. J. Appl. Meteorol. 40, 2178–2192.
Schmid, H.P., 1994. Source areas for scalars and scalar fluxes. Bound. Layer Meteorol. 67, 293–318.
Schmidt, H., Schumann, U., 1989. Coherent structure of the convective boundary layer derived from large-eddy simulations. J. Fluid Mech. 200, 511–562.
Schotanus, P., Nieuwstadt, F.T.M., de Bruin, H.A.R., 1983. Temperature measurement with a sonic anemometer and its application to heat and moisture fluxes. Bound. Layer Meteorol. 26, 81–93.
Stoy, P.C., Mauder, M., Foken, T., Marcolla, B., Boegh, E., Ibrom, A., Arain, M.A., Arneth, A., Aurela, M., Bernhofer, C., Cescatti, A., Dellwik, E., Duce, P., Gianelle, D., van Gorsel, E., Kiely, G., Knohl, A., Margolis, H., McCaughey, H., Merbold, L., Montagnani, L., Papale, D., Reichstein, M., Saunders, M., Serrano-Ortiz, P., Sottocornola, M., Spano, D., Vaccari, F., Varlagin, A., 2013. A data-driven analysis of energy balance closure across fluxnet research sites: the role of landscape scale heterogeneity. Agric. For. Meteorol. 171–172, 137–152.
Strunin, M.A., Hiyama, T., Asanuma, J., Ohata, T., 2004. Aircraft observations of the development of thermal internal boundary layers and scaling of the convective boundary layer over non-homogeneous land surfaces. Bound. Layer Meteorol. 111, 491–522.
Stull, R.B., 1988. An Introduction to Boundary Layer Meteorology. Kluwer Academic Publishers, Dordrecht.
Sühring, M., Raasch, S., 2003. Heterogeneity-induced heat flux patterns in the convective boundary layer: can the be detected from observations and is there a blending height? A large-eddy simulation study for the LITFASS-2003 experiment. Bound. Layer Meteorol. 148, 309–331.

Sun, J., Lenschow, D.H., Mahrt, L., Crawford, T.L., Davis, K.J., Oncley, S.P., MacPherson, I.J., Wang, Q., Dobosy, R.J., Desjardins, R.L., 1997. Lake-induced atmospheric circulations during boreas. J. Geophys. Res. 102, 29155–29166.
Taylor, C.M., Parker, D.J., Harris, P.P., 2007. An observational case study of mesoscale atmospheric circulations induced by soil moisture. Geophys. Res. Lett. 34, L15801.
Torrence, C., Compo, G.P., 1998. A practical guide to wavelet analysis. Bull. Am. Meteorol. Soc. 79, 61–78.
Townsend, A.A., 1961. Equilibrium layers and wall turbulence. J. Fluid Mech. 11, 97–120.
Träumner, K., Damian, T., Stawiarski, C., Wieser, A., 2014. Turbulent structures and coherence in the atmospheric surface layer. Bound. Layer Meteorol. 154, 1–25.
Turnipseed, A.A., Blanken, P.D., Anderson, D.E., Monson, R.K., 2002. Energy budget above a high-elevation subalpine forest in complex topography. Agric. For. Meteorol. 110, 177–201.
van Heerwaarden, C.C., Mellado, J.P., De Lozar, A., 2014. Scaling laws for the heterogeneously heated free convective boundary layer. J. Atmos. Sci. 71, 3975–4000.
van Heerwaarden, C.C., Vilà-Guerau de Arellano, J., 2008. Relative humidity as an indicator for cloud formation over heterogeneous land surfaces. J. Atmos. Sci. 65, 3263–3277.
Webb, E.K., Pearman, G.I., Leuning, R., 1980. Correction of flux measurements for density effects due to heat and water vapour transfer. Q.J.R. Meteorol. Soc. 106, 85–100.
Wilczak, J.M., Tillman, J.E., 1980. The three-dimensional structure of convection in the atmospheric surface layer. J. Atmos. Sci. 37, 2424–2443.
Williams, A.G., Hacker, J.M., 1993. Interactions between coherent eddies in the lower convective boundary layer. Bound. Layer Meteorol. 64, 55–74.
Wilson, K., Goldstein, A., Falge, E., Aubinet, M., Baldocchi, D., Berbigier, P., Bernhofer, C., Ceulemans, R., Dolman, H., Field, C., Grelle, A., Ibrom, A., Law, B.E., Kowalski, A., Meyers, T., Moncrieff, J., Monson, R., Oechel, W., Tenhunen, J., Valentini, R., Verma, S., 2002. Energy balance closure at FLUXNET sites. Agric. For. Meteorol. 113, 223–243.
Wulfmeyer, V., Branch, O., Warrach-Sagi, K., Bauer, H.S., Schwitalla, T., Becker, K., 2014. The impact of plantations on weather and climate in coastal desert regions. J. Appl. Meteorol. Climatol. 53, 1143–1169.
Ziv, B., Saaroni, H., Alpert, P., 2004. The factors governing the summer regime of the eastern mediterranean. Int. J. Climatol. 24, 1859–1871.